Albero V, Serra E, Espinós A, Romero ML, Hospitaler A. Internally fire protected composite steel-concrete slim-floor beam. Engineering Structures 2021; 227:111447. https://doi.org/10.1016/j.engstruct.2020.111447

Internally fire protected composite steel-concrete slim-floor beam

V. Albero [a,b*], E. Serra [b], A. Espinós [b], M. L. Romero [b], A. Hospitaler [b]

[a]*Department of Mechanical Engineering and Construction, Universitat Jaume I, Castellón, Spain*
[b]*Instituto de Ciencia y Tecnología del Hormigón (ICITECH), Universitat Politècnica de València, Valencia, Spain*
** Corresponding author. e-mail address: valbero@uji.es*

ABSTRACT

The slim-floor beam is a composite concrete-steel beam fully integrated into the floor depth that was developed at the beginning of the 1990s. This composite beam presents a very good behaviour during the fire event because most of the steel parts of the section remain protected by the concrete encasement. Indeed, in a fire event, only the bottom surface of the lower steel plate results exposed to the heat source. The use of intumescent coating or other fireproof materials is the most common way to insulate the steel beam from fire but requires an accurate application and also appropriate maintenance during its whole life cycle to ensure proper fire protection. Thus, related to this last idea, the objective of this work is to present a new slim-floor configuration which increases the insulation of the beam from fire by using a design strategy that avoids the needed for maintenance. This new beam configuration has been called “Internally Fire Protected Slim-Floor Beam” (IFP-SFB) and implies a thermal break included within the beam cross-section. This paper presents the results of a series of thermal tests applied to this innovative slim-floor type proposed by the authors and its comparison against the most commonly used slim-floor configurations. Finally, the benefits of the proposed IFP-SFB configuration are presented, resulting in up to 30-60 minutes of additional fire resistance time. The IFP-SFB configuration is at present right-protected and under evaluation by the Spanish Office of Patents and Trademarks with reference number P201930438.

Keywords*: Steel-concrete composite beams, fire resistance, slim-floor beam, electric furnace, thermal experiments, fire protection, shallow floor beam, integrated floor beam.*

1 INTRODUCTION

The fire action is one of the most important hazards that may affect any structural element. During the last decades, specific provisions have been incorporated into structural standards around the world to take into account this accidental load [1-4]. Many researchers have been working on this topic during the second half of the twentieth century and significant advances have been done conductive to improve the fire safety in buildings.

Regarding this subject, it is worth mentioning that composite concrete-steel structural members have demonstrated a good behaviour against fire as compared with bare steel members, which are highly affected by the elevated temperatures produced during the fire event. For instance, composite steel-concrete columns like concrete-filled steel Tubular columns have showed a very good fire behaviour due to the synergy of the steel tube and the concrete core working together [4-7]. Additionally, recent studies [8-21] have confirmed a promising behaviour at elevated temperatures of the slim-floor beam.

The so-called slim-floor beam is a type of composite beam made up by an I-section welded to a bottom steel plate, which was developed by the most important steel manufacturers as *ArcelorMittal*, *Peikko*, *Tata Steel*, etc. Specifically, two different slim-floor beam configurations are available in market: The Shallow Floor Beam (SFB), made by a complete I-section welded to a bottom plate (Fig. 1a), and the Integrated Floor Beam (IFB), which consists of a half I-section also welded to a bottom plate (Fig. 1b). The slim-floor beam configuration provides a plain supporting surface which allows for an easy and fast erection of different floor systems like steel composite floor decks or precast concrete slabs. Moreover, the slim-floor

main steel beam remains fully embedded into the concrete floor depth, thus providing a thinner (slim) floor and a clear lower surface which permits the easy installation of under-floor technical equipment, see Fig. 1c.

Concerning the fire performance of this system, the slim-floor beam presents a very good behaviour during fire, since the steel beam is totally embedded into the concrete floor and therefore it results only exposed to fire from its lower surface. Owing to this configuration, the temperature within the steel members of the section increases slower than in other steel or composite concrete-steel beams, which are most frequently exposed to fire from the three sides. Additionally, recent research studies [8], [16] have proved that the SFB configuration, which is formed by a double steel sheet at the bottom part -lower flange of the steel profile and bottom plate, see Fig. 1a-, shows a very good thermal behaviour during fire. Specifically, this finding was deduced on a previous experimental program developed by authors [16], which consisted of eight thermal experiments. These thermal experiments were focused on the study of different cross-section changes like the lower steel plate thickness, the usage of innovative materials or the behaviour of IFB and SFB configuration. The interesting fire behaviour observed by the SFB configuration can be explained by the action of a thermal gap which appears at the contact interface between the bottom plate and the I-section lower flange due to its thermal bow, see Fig. 2. It has been experimentally confirmed that the thermal gap across this interface allows for a temperature delay up to 100ºC in the I-section lower flange [16]. This thermal gap was also observed by Both et al [9] who even proposed to increase this gap during the manufacturing process. The described benefits of the thermal gap on the SFB beams suggested the authors to improve the thermal behaviour of this slim-floor beam by increasing this gap using any insulation material.

In turn, the thermal behaviour of steel beams in fire can be also enhanced by using fireproof materials. Indeed, the usage of protection coatings like intumescent paint is the most

common way to protect bare steel structural members. This type of coating reacts during the temperature range between 200-400ºC creating an expansive insulation layer that protects the steel from the heat source. Additionally, other fireproof materials like spray-applied vermiculite are also available to provide a similar fire protection.

Anyhow, all of these protection materials, which are directly placed at the exposed surface, remain exposed to ambient conditions during their whole life cycle. This persistent exposure to aggressive ambient condition – as it is the case of industrial buildings – may affect their fireproofing action. Indeed, recent research studies [22] have demonstrated the negative effect of the aging on the intumescent coatings due to a lower expansion ratio and worse insulation. Therefore, fire protection materials not only require an accurate application, but also an appropriate maintenance during their whole life cycle to ensure a proper fire protection.

Related to this last idea, the main objective of this paper is to present a new slim-floor beam configuration designed to increase the insulation of this composite system against fire by using a new strategy that, among other benefits, does not needed for maintenance. This new beam configuration has been called by the authors "*Internally Fire Protected Slim-Floor Beam*" (IFP-SFB) because, as it is described in the following sections, the fire protection is not placed at the outer surface of the cross-section but within the section itself, thus it does not result directly exposed to ambient conditions. This paper also presents the results of an experimental campaign carried out at the *Universitat Politècnica de Valencia* (Spain) testing facilities, focused on the thermal behavior of this new IFP-SFB configuration. The mechanical behavior of this innovative slim-floor beam configuration at elevated temperatures is also assessed and compared with the most common slim-floor beam types in terms of fire resistance.

2 INTERNALLY FIRE PROTECTED SLIM-FLOOR BEAM (IFP-SFB)

2.1 Description of the IFP-SFB configuration

The Internally Fire Protected Slim-Floor Beam (IFP-SFB) presented in this paper consists of an I-section steel profile welded to a wider bottom steel plate with an insulation layer of 5mm thick placed in between the two, see Fig. 3. This insulation layer is made up of a flexible and non-combustible material, which protects the I-section profile from the temperature rise through its bottom surface. The here presented IFP-SFB configuration is at present right-protected and under evaluation by the Spanish Office of Patents and Trademarks with reference number P201930438.

This insulation layer remains placed in a cavity created on purpose between the bottom plate and the lower flange of the steel profile thank to the weld between them. Therefore, the insulation material is totally protected from any aggressive ambient conditions and no maintenance is required. This insulation layer is made of a material which shows a density between 200-400 kg/m^3, a thermal conductivity lower than 0.08 W/m·K at 600ºC and a specific heat value around 1000 J/Kg·K. Besides, this material is flexible enough to follow any deflection of the bottom plate without showing any crack.

2.2 IFP-SFB manufacturing process

The manufacturing process of the IFP-SFB can be summarized into three steps. The first step consists of the bottom plate conditioning and alignment to receive the insulation layer. Two square bars are placed to mark the edge of the insulation layer, see Fig. 4a. The second step consists of placing the insulation layer over the bottom plate, see Fig. 4b. The square bars result useful to achieve a correct alignment of the insulation layer without applying any adhesive that may create combustion problems. Finally, in the third step the I-section steel profile is directly

placed over the insulation layer and two continuous welding lines, one at each side, are created to join the lower flange of the steel profile to the bottom steel plate, see Fig. 4c.

It is worth to be noticed here that, as it can be seen in the detail of Fig. 4c, the weld action melts the steel material but has no significative effect over the insulation layer non-combustible material. The welding line must be thick enough to create a proper assembly, following the construction practice.

The manufacturing process described above seems easy enough to be standardized in the current automated manufacturing steel factories. The novelty of this process comes mainly from the insulation layer placement, but the rest of the process does not differ significantly from the current manufacturing scheme.

2.3 IFP-SFB behaviour at room temperature

As it was described above, the main difference between the presented IFP-SFB and the traditional SFB configuration consists of adding an insulation layer in-between the two steel plates. An enhanced fire behaviour of this beam cross-section is expected due to the insulation layer. However, it should be also ensured that the behaviour at room temperature is not affected.

Indeed, the first experimental test carried out using the new IFP-SFB configuration was focused on the room temperature behaviour under pure bending conditions. Specifically, two bare specimens of 6 m long, made up of a HEB200 steel profile welded to a bottom plate of 360 mm wide and 15 mm thick, were tested at the *Universitat Politècnica de Valencia* testing facilities. The steel grade of both beams was S355. One of these specimens was configured as the common SFB beam while the other one included the insulation layer following the previously described IFP-SFB configuration. Both specimens were subjected separately to a four-point bending test in order to assess their flexural behaviour at room temperature, see Fig. 5. The four-point bending test setup ensures the failure in pure bending at the mid-length section

without any shear force interaction. The real span of the beam test configuration was 5.8 m given the layout of the supports, which consisted of rigid rollers, see Fig. 5a.

The tests were instrumented using 3 LVDTs to measure the beam deflection and 7 strain gauges to control the longitudinal strains along the mid-length section height, see Fig. 5a and Fig. 6b. The results of these two experiments, SFB and IFP-SFB, are shown in terms of applied load versus mid-length deflection in Fig. 6a. Both experiments presented almost identical results and showed a well-defined elastic-plastic behaviour with the same maximum applied load of P_{pl} = 320 kN.

The end of the elastic behaviour was observed when reaching about 250 kN of applied load, which matches with the obtained value from the beam theory, given the SFB cross-section properties: elastic modulus W_{el} = 652723 mm^3 and yield strength f_y = 355 MPa. These values give an elastic bending moment of M_{el} = 231,7 mkN, which under the four-point bending test scheme described in Fig. 5a fit with an applied load of 240,1 kN.

One important finding result from this particular analysis is that the IFP-SFB configuration allows for the full development of the cross-section plastic resistance, achieving the same maximum applied load as the conventional SFB cross-section. Therefore, the addition of the insulation layer does not compromise the flexural capacity of the section at room temperature. Only a slight difference was observed on the beam stiffness evolution during the elastic range, Fig. 6a, due to the slightly higher height of the IFP-SFB beam, necessary to accommodate the insulation layer.

Finally, Fig. 6b shows the longitudinal strain distribution along the cross-section in the elastic range (P = 150 kN), where the Euler-Bernoulli linear distribution of strains can be clearly observed. The most relevant fact to be highlighted in Fig. 6b is that no slip is observed between the bottom steel plate and lower flange of the I-profile, according to the measurements of the strain gauges on the IFP-SFB specimen. This fact means that the IFP-SFB configuration does

not present any problem on the load transfer at the weld between the bottom plate and lower flange of the I-profile and thus the full bending resistance of the cross-section can be achieved.

3 BEHAVIOUR OF IFP-SFB AT ELEVATED TEMPERATURES: THERMAL TESTS

3.1 Experimental campaign

The experimental campaign presented in this section was carried out at the fire testing facilities of the *Universitat Politècnica de Valencia*, Spain. It was focused on the thermal behaviour of the previously described Internally Fire Protected slim-floor beam at elevated temperatures. This experimental campaign continues the eight thermal tests presented in [16] which analysed the slim-floor beam thermal behaviour and the application of the most common protection systems against fire like the usage of intumescent coating.

Specifically, three new specimens were tested here in order to assess the thermal behaviour of the new and innovative IFP-SFB slim-floor configuration, see Table 1. The first specimen (S1) follows the common SFB configuration and was used as a reference experiment for comparison. This specimen was made up with an HEB200 steel profile welded to a 15x360 mm bottom plate. Hollow core slabs were used as the secondary element for the floor system and an in-situ concrete topping of 5 cm thick was added to achieve a total floor height of 250 mm. Moreover, two reinforcing bars of 20 mm diameter were embedded within the concrete mass with 30 mm cover measured from the top face of the lower steel flange and placed at a distance of 40 mm to the profile web.

The second specimen (S2) was identical to the first one, with the only difference of adding the insulation layer described in section 2 in-between the two steel plates (see Fig. 7), generating the so-called Internally Fire Protected slim-floor beam which is the object of study in this work.

Finally, the third specimen (S3) was equal to S2 but in this case with a bottom plate made up of austenitic stainless steel grade 1.4301 (AISI 340). The reason behind this test comes from recent research studies [23], [24] that have demonstrated the improved fire behaviour of stainless steel. This test pretends to assess the combined effect, in terms of fire protection, of the insulation layer and the beneficial behaviour of stainless steel at elevated temperature.

The steel parts used in all the test specimens were grade S355, having a nominal yield strength of 355 MPa, the nominal compressive strength (cylindrical) of the cast in-situ concrete was 30 MPa and the precast concrete hollow core slabs were manufactured with 45 MPa nominal compressive strength (cylindrical). In turn, the embedded reinforcing bars were grade S500, with 500 MPa nominal yield strength.

Owing to the standard furnace for fire test is no longer available in our testing facilities, the thermal tests were carried out using an electric furnace made of four radiative panels of 3kW each manufactured with electric wires embedded in ceramic bricks. The radiative panels were placed creating a rectangular furnace with dimensions1020 mm wide, 1800 mm long and 510 mm high. The configuration of panels permits that the specimens are placed at the open top surface, see Fig. 8. Therefore, the slim-floor beam remains exposed to the heat source from its lower surface, as it is the case of real fire conditions.

The power and configuration of the testing furnace described above allows that temperatures up to 800ºC can be reached inside the chamber. In order to measure the temperature evolution along the slim-floor cross-section, four type-K thermocouples were placed within the specimen. Specifically, thermocouple TC1 registers the temperature evolution at the bottom steel plate; TC2 measures the lower flange temperature; TC3 is placed at the web of the steel profile and TC4 measures the evolution of the reinforcing bar temperature, see Fig. 7. The furnace temperature (TF) is also controlled by using four plate-thermocouples placed into the chamber. The control device was set up to reach automatically a target temperature of

800ºC at the maximum allowed heating rate. The specimens were kept inside the furnace during 240 minutes. The temperature registered into the furnace (TF) and in thermocouples TC1 to TC4 is shown in Table 2 in steps of 30 minutes.

The temperature results from the tests are also displayed in Fig. 9. Specifically, Fig. 9a shows the evolution of thermocouples TC1 and TC2 during the three experiments. It can be observed that the difference between TC1-TC2, which shows the temperature gap between bottom plate and lower steel flange, increases from S1 to S2 and also from S2 to S3, see black arrows in Fig. 9a. Additionally, it is worth reminding here that specimen S1 was configured as the common slim-floor SFB while specimen S2 is the IFP-SFB slim-floor presented in this work. Therefore, the effect of the insulation layer placed into the cavity between bottom plate and lower steel flange results enough to increase the temperature gap up to 200ºC. Specimen S3 which includes stainless steel at the bottom steel plate increases the temperature gap up to 250ºC. It can be concluded that IFP-SFB configuration creates a heating delay that permits a slower temperature increment of the lower steel flange. This delay is even higher when the bottom plate is made of stainless steel, due the positive effect of the lower emissivity and conductivity of this material. However, it is also true that due to the position of the insulation layer the bottom plate temperature increases slightly faster than in specimen S1.

In turn, Fig. 9b shows the temperature evolution of the steel profile web (TC3) and reinforcing bars (TC4). Both thermocouples show a slower increase of the temperature in case of S2 and S3 specimens, which are internally fire protected.

The results obtained in these tests confirm that internally fire protected specimens (S2 and S3), show a promising thermal response resulting in lower temperatures along the key steel parts of the cross-section. As it was explained before, due to the standard furnace for fire test is no longer available in our testing facilities, the subsequent necessary steps to confirm the enhanced fire behaviour of this novel slim-floor configuration consists of the development of a

finite element thermal model in order to evaluate the fire performance of this new configuration when it is exposed to a standard ISO834 time-temperature curve, as well as the assessment of the mechanical response of the cross-section at elevated temperature.

3.2 Finite element thermal model

A finite element (FE) model was developed, capable to simulate the transient heat transfer problem on slim-floor cross-sections exposed to elevated temperatures. This numerical model was developed using the commercial nonlinear finite element analysis package ABAQUS [25]. The FE model presented here was already described and validated by authors in previous works [8], [16]. The main characteristics of this FE model are summarized here in order to evaluate its performance on *the Internally Fire Protected* configuration.

The main objective of the FE model consists of solving the temperature *(θ)* evolution along the slim-floor cross-section through the *Fourier's* heat transfer differential equation:

$$\nabla(\boldsymbol{k} \cdot \nabla\theta) = \rho c_p \frac{\partial\theta}{\partial t} \quad (1)$$

The thermal material properties implicit in this equation are: Thermal conductivity (**k**); specific heat (c_p) and material density (ρ). These material properties are temperature dependent and were obtained for concrete and steel in composite structures from EN 1994-1-2 [1]. In particular, for the concrete specific heat, a 4% of moisture content for the peak value was established and the upper conductivity level was assumed. In case of stainless steel, for specimen S3, the thermal material properties from EN1993-1-2 Annex C [3] were used.

Taking as a reference the insulation silicate-fibre materials currently available in market, the insulation layer used in specimens S2 and S3 was defined by a conductivity value of 0.08 W/m·K at temperatures lower than 600ºC and 0.17 W/m·K at temperatures higher than 1000ºC. Between 600 and 100ºC, a linear interpolation function is defined. The specific heat of this insulation material was defined with a value of 1000 J/kg·K and the density was 300 kg/m^3.

The slim-floor cross-section was meshed by using 2D four-noded quadrilateral elements. The maximum mesh size was 5 and 2.5 mm for the concrete and steel parts respectively, see Fig. 10. The reason behind this finer mesh on the steel members comes from the higher importance of this parts in the general bending behaviour. Thus, a more accurate temperature prediction needs to be obtained.

Regarding the heat convection and radiation, this heat transfer mechanisms were taken into account as boundary conditions in both the bottom 'exposed' and the upper 'unexposed' surfaces. These conditions are defined as follows:

$$-\boldsymbol{n} \cdot \boldsymbol{k} \cdot \nabla\theta = h\,(\theta - \theta_\infty) + F \cdot \varepsilon \cdot \sigma\,(\theta^4 - \theta_\infty^4) \quad (2)$$

In this equation, the emissivity -ε- value for the heat radiation was taken, following from EN1994-1-2 [1], as 0.7 for the concrete and carbon steel surfaces, while for the stainless steel surface (specimen S3) a value of 0.4 was used, following from EN 1993-1-2 Clause 2.2 [3]. In turn, the convective coefficient -h- was defined as 25 W/m^{2}K at the exposed surface and 4 W/m^{2}K at the unexposed one, following from EN 1991-1-2 [26]. The view factor -*F*- and the normal vector -**n**- at the boundary surface were automatically computed by ABAQUS. Finally, the temperature -θ_∞- represents the fire action as a time-temperature curve. This fire action was assumed as the furnace time-temperature evolution (TF) for the FE model validation. However, for the standard fire resistance assessment, the standard ISO-834 time-temperature curve was used.

Additionally, the contact properties at the interface between different materials should be defined in the thermal FE model. Specifically, according to previous works from the authors [8], [16] a thermal conductance value of 250 W/m^{2}K was assumed for the concrete-steel interaction, while a value of 100 W/m^{2}K was established for the steel-steel contact. It is worth to be mentioned here that the steel-steel thermal contact between bottom plate and lower steel flange in specimen S1 is substituted by the insulation layer in specimens S2 and S3.

Finally, the developed FE model was used to reproduce the experiments described in the previous subsection. The numerical and experimental results at the available thermocouple locations are displayed in Fig. 11 and Table 2. As it can be seen, the FE model showed a very good agreement with the experimental measurements with a total mean error value of 1.03 which lies on the safe side and a standard deviation rate of 0.11. Therefore, it can be concluded that the developed FE thermal model permits the assessment of the *Internally Fire Protected* slim-floor configuration against the standard ISO-834 time-temperature curve in order to obtain its standard fire resistance, which will be done in the following section.

4 MECHANICAL BENDING RESISTANCE UNDER STANDARD FIRE CONDITIONS

Once the thermal model was validated against the previously described experiments, the three configurations listed in Table 1 (SFB, IFP-SFB and IFP-SFB with stainless steel bottom plate) were computed numerically under a standard ISO-834 time-temperature curve. In this way, the temperature field (θ_i) evolution along the slim-floor cross-section was available for the three cases.

Subsequently, the bending moment plastic resistance at elevated temperatures ($M_{pl,Rd,\theta}$) was obtained by an iterative incremental analysis, previously described by the authors in [16]. This analysis considers the non-linear mechanical behaviour of concrete and steel at elevated temperatures. Specifically, the elevated temperature constitutive models available in EN1994-1-2 [1] and EN1993-1-2 [3] were used for concrete and steel respectively. Besides, it should be noticed that the constitutive model for stainless steel at elevated temperatures was adopted from EN1993-1-2 [3] Annex C. Additionally, it should be highlighted that a full composite action was numerically taken into account between the concrete slab and top steel flange, which simulated the effect of the shear connectors.

The previously mentioned iterative process consists of the increase of the reference point strain (ε_0) and the cross-section curvature (χ_y) until the mechanical equilibrium is fulfilled:

$$\begin{bmatrix} \delta N_{Rd,\theta} \\ \delta M_{pl,Rd,\theta} \end{bmatrix} = \begin{bmatrix} E_{11} & E_{12} \\ E_{21} & E_{22} \end{bmatrix} \cdot \begin{bmatrix} \delta\varepsilon_0 \\ \delta\chi_y \end{bmatrix} \quad (3)$$

In this equilibrium equation, the non-linear behaviour of the materials is taken into account through (E_θ) and the specimens are considered as axially unrestrained. The external net axial force is fixed as $\delta N_{Rd,\theta} = 0$.

The secant stiffness matrix for each increment can be obtained by dividing the slim-floor beam cross-section into cells matching with the FE elements, where the temperature evolution (θ_i) was obtained from the previous thermal analysis:

$$E_{11} = \sum E_{\theta,i}\, A_i;\; E_{12} = E_{21} = \sum E_{\theta,i}\, y\, A_i;\;\; E_{22} = \sum E_{\theta,i}\, y_i^2\, A_i \quad (4)$$

The incremental analysis is computed by increasing the curvature (χ_y) until the maximum value of the bending moment is achieved or the stiffness matrix becomes singular. Following from this procedure, a non-linear $M - \chi$ curve is obtained for each specimen and fire exposure time. The temperature field within the slim-floor cross-section and stress distribution along the beam height for each material part during the failure stage can be observed in Fig. 12.

Additionally, the thermal strains (ε_{th}) were considered by substracting them from the total strain before solving the equilibrium equation. Moreover, it should be noticed that thermal strains do not provide net external axial force, since the specimens were axially unrestrained. However, a null internal curvature (χ_y) generates a non-zero bending moment due to the effect of the thermal strains (ε_{th}).

The plastic bending moment resistance of specimens S1, S2 and S3 from Table 1 is displayed in Fig. 13 and Table 3 under different standard ISO-834 times. The improvement of fire resistance achieved by IFP-SFB, with or without stainless steel (S2, S3 specimens), can be

easily observed when compared against SFB (S1) specimen. However, it should be noticed that during the first stages of fire, with exposures lower than 30 minutes, S3 specimen with stainless steel shows a slightly lower flexural resistance. The reason behind this fact comes from the higher loss of strength suffered by stainless steel at temperatures lower than 400-500ºC following the model in EN1993-1-2 [3] Annex C. However, for temperatures higher than 500ºC the reduction factors of the stainless steel mechanical properties remain higher than those of normal steel, resulting in a better performance for higher fire exposures.

In any case, it is observed that in general, under the same bending moment applied, S2 and S3 configurations show higher fire resistance times. Specifically, under approximately a 40% of the bending moment resistance at room temperature, the SFB configuration shows 60 minutes of fire resistance, while IFP-SFB increases this fire endurance up to 90 minutes and even up to 120 minutes with bottom plate made of stainless steel (S3). Therefore, under a 40% of load level - which is a frequent value in fire design - the new type of beam proposed in this work increases 30 minutes the fire resistance time and even 60 additional minutes when the bottom plate is made of stainless steel.

5 CONCLUDING REMARKS

This work has presented an innovative slim-floor beam cross-section configured to increase the fire endurance of this system. This new slim-floor configuration has been called "*Internally Fire Protected Slim-Floor Beam*" (IFP-SFB), since the fire protection consists of an insulation layer placed between the SFB bottom steel plate and the lower steel flange of the steel profile. Thus, the insulation layer remains protected from external agents with no need for maintenance.

The experimental tests carried out in this work confirmed that the insulation layer delays the temperature increase of the steel profile and the reinforcing bars embedded within the slim-floor cross-section. Specifically, 200ºC temperature difference between bottom plate and lower

steel flange can be reached and the reinforcing bars temperature drops up to 100ºC when compared with the common SFB configuration.

This general temperature decay in the section produces an important improvement of the mechanical behaviour of the slim-floor beam in fire. The proposed IFP-SFB configuration has shown an increase of 30 minutes of fire resistance at 40% load level as compared with the common SFB type. Additionally, the use of stainless steel at the bottom plate can enhance even more this beneficial fire behaviour, increasing the fire resistance of the system up to 120 minutes at the referred 40% load level.

In conclusion, the innovative IFP-SFB configuration proposed in this paper may become a promising idea to be exploited by manufactures in the application of slim-floor beams, making possible to achieve an additional fire endurance.

ACKNOWLEDGEMENTS

The authors would like to express their sincere gratitude to the Spanish "Ministerio de Economía y Competitividad" for the help provided through the Project BIA2015-67192-R and to the European Union through the FEDER funds.

The here presented "*Internally Fire Protected Slim-Floor Beam*" (IFP-SFB) configuration is currently right-protected and under evaluation by the Spanish Office of Patents and Trademarks with the reference number P201930438 and with publication number ES2732719 A1.

REFERENCES

[1] CEN, EN 1994-1-2, Eurocode 4: Design of composite steel and concrete structures. Part 1-2: General rules - Structural fire design., Comité Européen de Normalisation, Brussels, Belgium, 2005.

[2] CEN, EN 1992-1-2, Eurocode 2: Design of concrete structures. Part 1-2: General rules – Structural fire design., Comité Européen de Normalisation, Brussels, Belgium, 2004.

[3] CEN, EN 1993-1-2, Eurocode 3: Design steel structures. Part 1-2: General rules - Structural fire design., Comité Européen de Normalisation, Brussels, Belgium, 2005.

[4] Kodur VKR, Mackinnon DH. Design of concrete-filled hollow structural steel columns for fire endurance. Engineering Journal. 2000;37:13-24.

[5] Han LH, Zhao XL, Yang YF, Feng JB. Experimental study and calculation of fire resistance of concrete-filled hollow steel columns. Journal of Structural Engineering. 2003;129:346-56.

[6] Romero ML, Espinós A, Renaud C, Bihina G, Schaumann P, Kleiboemer P et al. Fire resistance of innovative and slender concrete filled tubular composite columns (FRISCC). Final Report, Catalogue number KI-NA-28082-EN-N. RFCS Publications. Brussels 2016.

[7] Romero ML, Espinós A, Lapuebla-Ferri A, Albero V, Hospitaler A. Recent developments and design provisions for concrete-filled steel tubular columns and slim-floor beams. Journal of Constructional Steel Research. 2020 *(Under review)*

[8] Albero V, Espinós A, Serra E, Romero ML, Hospitaler A. Numerical study on the flexural behaviour of slim-floor beams with hollow core slabs at elevated temperature. Engineering Structures. 2019;180:561-73.

[9] Both C, Fellinger JHH, Twilt L. Shallow floor construction with deep composite deck: From fire tests to simple calculation rules. Heron. 1997; 42(3):145-158.

[10] Romero ML, Albero V, Espinós A, Hospitaler A. Fire design of slim-floor beams. Stahlbau. 2019;88:665-74.

[11] Romero ML, Cajot LG, Conan Y, Braun M. Fire design methods for slim-floor structures. Steel Construction. 2015;8:102-9.

[12] Newman GM. Fire resistance of slim floor beams. Journal of Constructional Steel Research. 1995;33:87-100.

[13] Kim HJ, Kim HY, Park SY. An experimental study on fire resistance of slim floor beam, Applied Mechanics and Materials. 2011:752-757.

[14] Ma A, Mäkeläinen P. Structural behaviour of composite slim floor frames in fire conditions. Journal of Constructional Steel Research. 2006;62(12):1282-1289.

[15] Zaharia R, Franssen JM. Simple equations for the calculation of the temperature within the cross-section of slim floor beams under ISO Fire. Steel and Composite Structures. 2012;13:171-85.

[16] Albero V, Serra E, Espinós A, Romero ML, Hospitaler A. Innovative solutions for enhancing the fire resistance of slim-floor beams: Thermal experiments. Journal of Constructional Steel Research. 2020;165:105897.

[17] Hanus F, Zaganelli D, Cajot L-G, Braun M. Analytical methods for the prediction of fire resistance of "reinforced" slim floor beams. In: Sohn E, editor. EuroSteel 2017. Copenhagen, Denmark 2017.

[18] Mäkeläinen P, Zhongcheng M. Fire resistance of composite slim floor beams, Journal of Constructional Steel Research. 2000; 54(3): 345-363.

[19] Shahabi SEM, Ramli Sulong NH, Shariati M, Mohammadhassani M, Sha SNR. Numerical analysis of channel connectors under fire and a comparison of performance with different types of chear connectors subjected to fire, Steel and Composite Structures. 2016; 20(3): 651-669.

[20] Davoodnabi SM, Mohammad Mirhosseini S, Shariati M. Behaviour of steel-concrete composite beam using angle shear connectors at fire condition, Steel and Composite Structures. 2019; 30(2): 141-147.

[21] Romero ML, Espinós A, Lapuebla-Ferri A, Albero V, Hospitaler A. Recent developments and fire design provisions for CFST columns and slim-floor beams. Journal of Constructional Steel Research. 2020; 172:106-159.

[22] Li GQ, Xu Q, Wang L, Han J, Main issues on behaviour of intumescent coatings. Keynote Lecture, Applications of Structural Fire Engineering conference. ASFE 2019. Singapore.

[23] Gardner L, Insausti A, Ng KT, Ashraf M. Elevated temperature material properties of stainless steel alloys, Journal of Constructional Steel Research. 2010;66(5):634-647.

[24] Chen J, Young B. Stress–strain curves for stainless steel at elevated temperatures, Engineering Structures. 2006; 28(2): 229-239.

[25] ABAQUS, Abaqus/Standard Version 6.14 User's Manual: Volumes I-III, Pawtucket, Rhode Island: Hibbit, Karlsson & Sorensen, Inc (2014).

[26] CEN, EN 1991-1-2, Eurocode 1: Actions on structures. Part 1-2. General actions - actions on structures exposed to fire, Comité Européen de Normalisation, Brussels, Belgium, 2002.

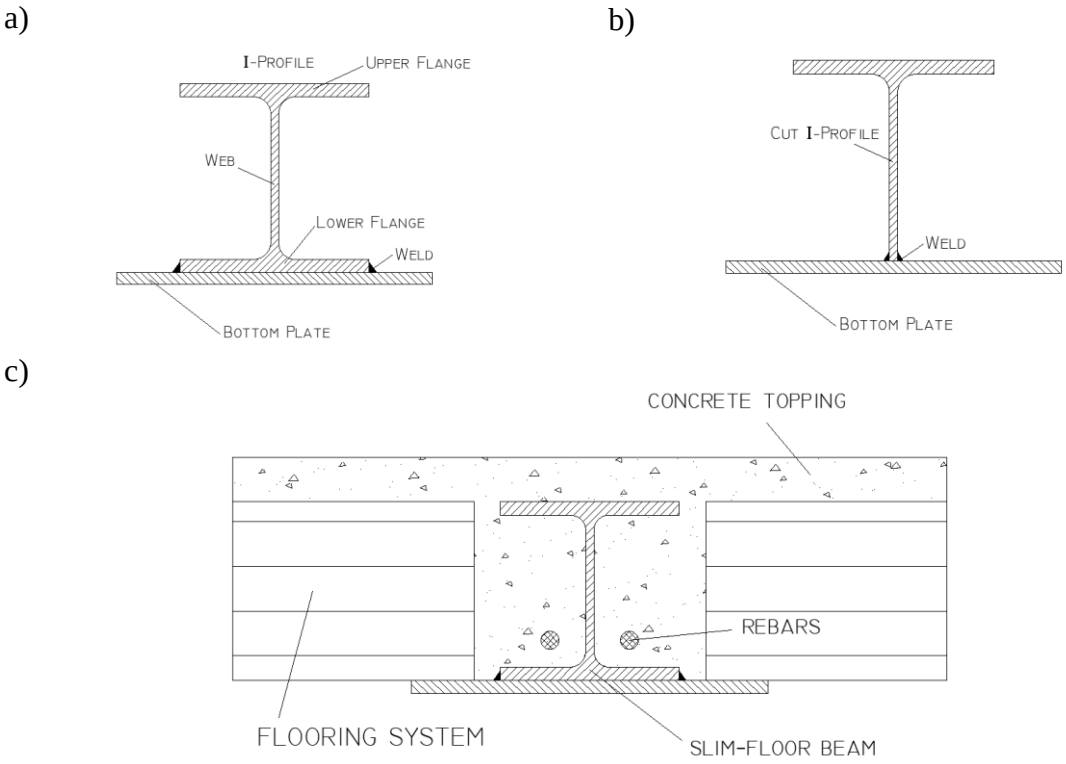

Fig. 1. a) Shallow Floor Beam (SFB). b) Integrated Floor Beam (IFB). c) Slim-floor system

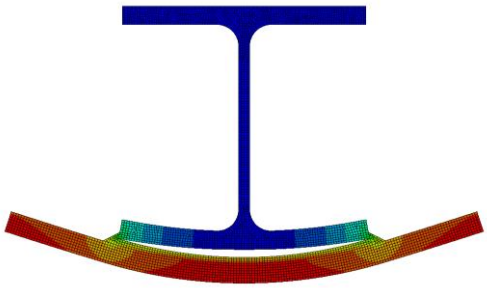

Fig. 2. SFB thermal bow.

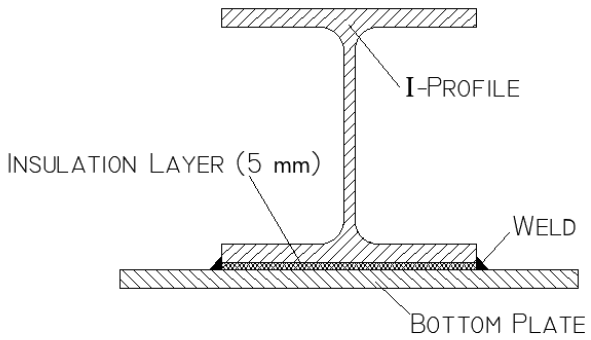

Fig. 3. Internally Fire Protected Slim-Floor Beam (IFP-SFB)

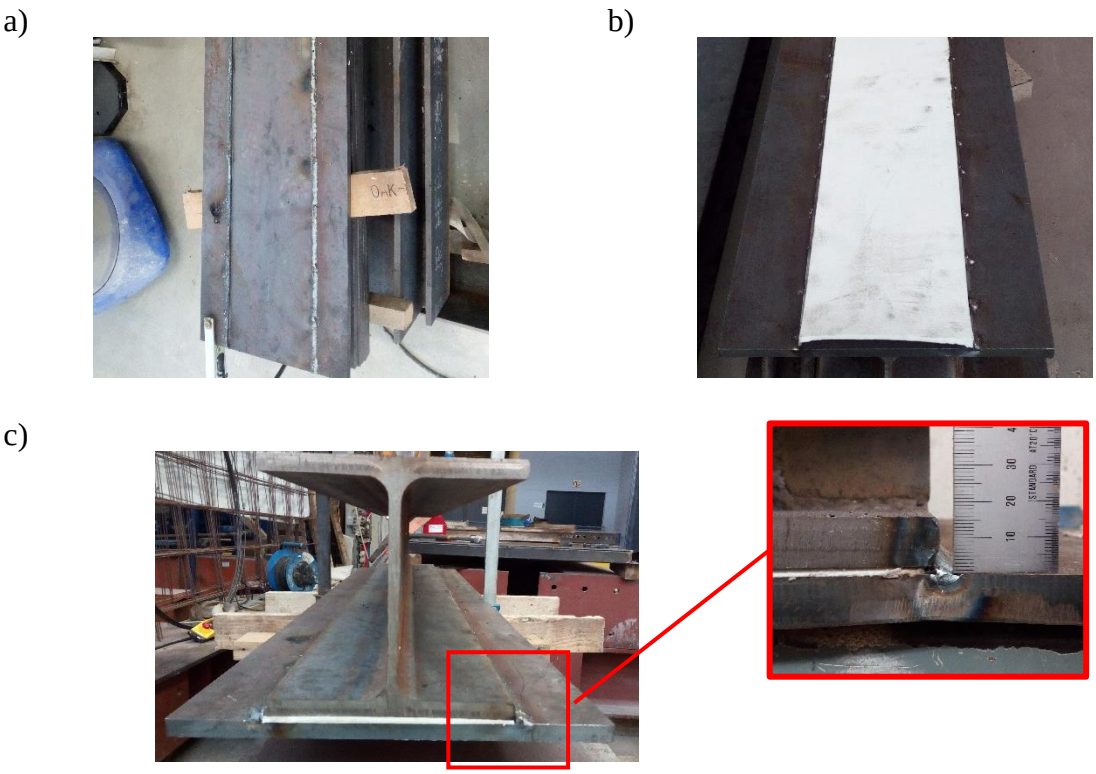

Fig. 4. IFP-SFB manufacturing process. a) Bottom plate conditioning. b) Insulation layer fitting. c) Final look of the section (weld detail)

a)

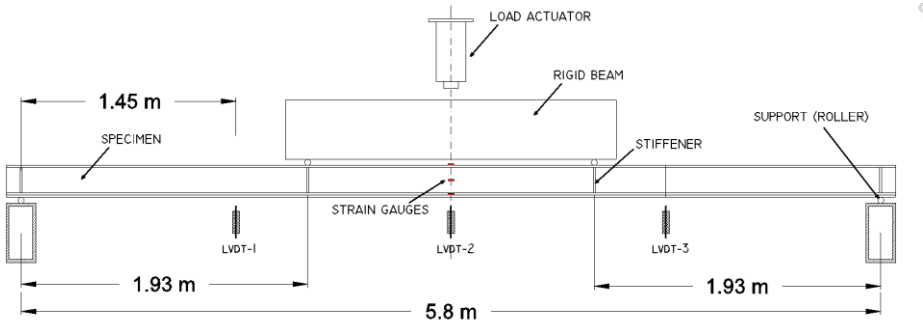

b)

Fig. 5. Four-point bending test at room temperature. a) Schematic view of the test setup. b) General and lateral view.

a)

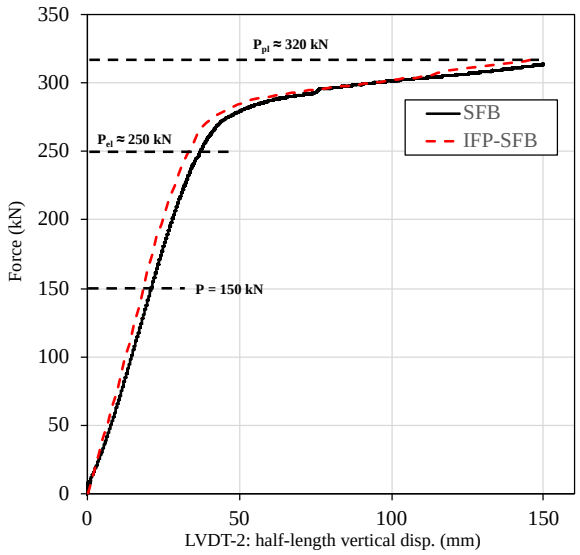

b)

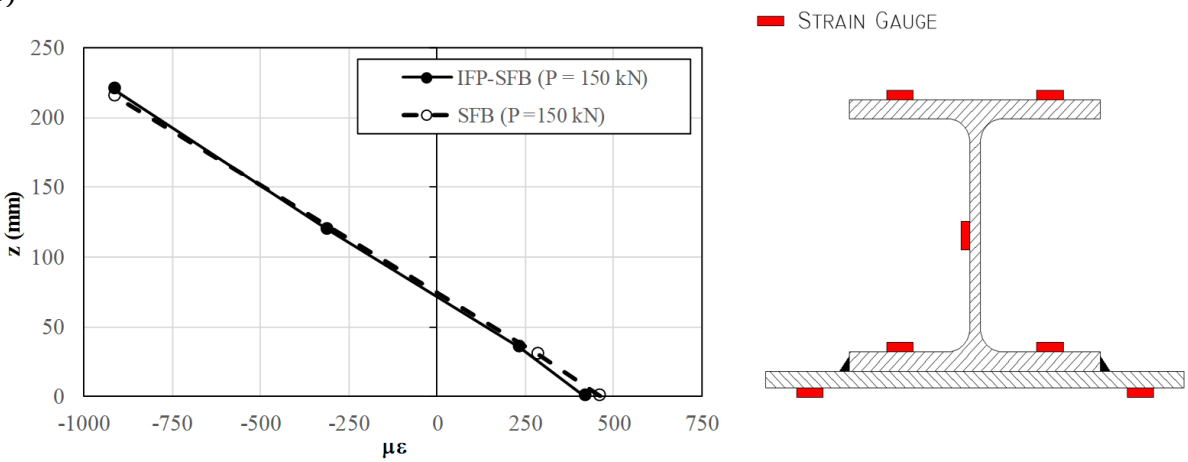

Fig. 6. Room temperature test results. a) Load vs. mid-length displacement. b) Longitudinal strain field across the section at linear elastic range (P = 150 kN)

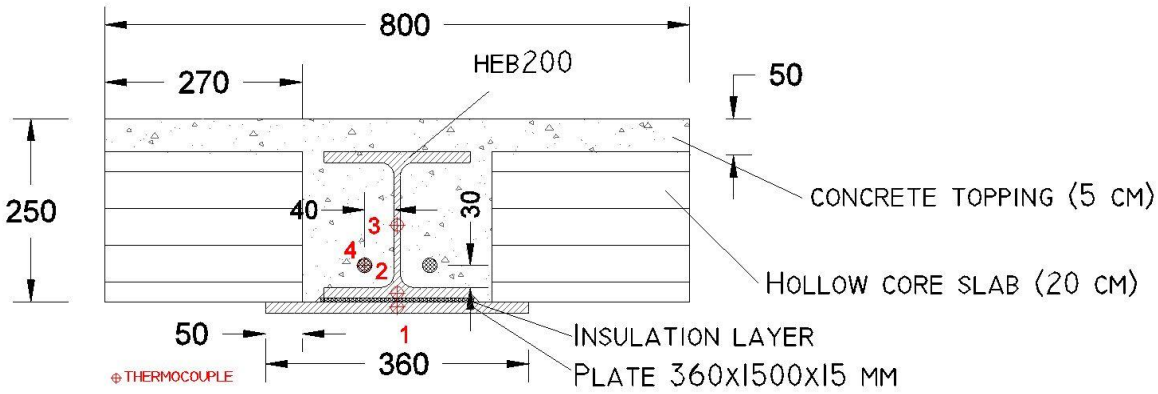

Fig. 7. S2 specimen layout

Fig. 8. Test setup for the thermal experiments in electric furnace.

a)

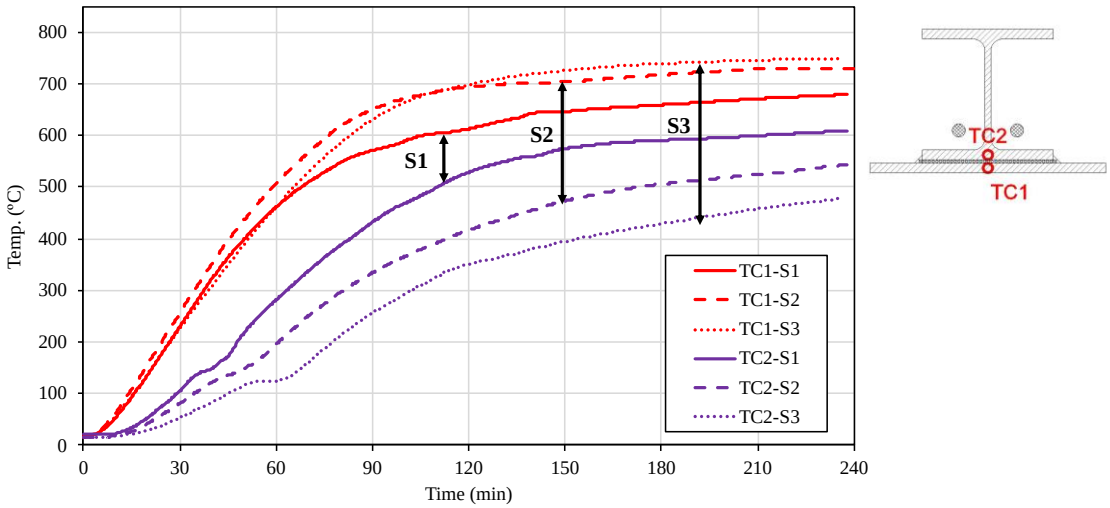

b)

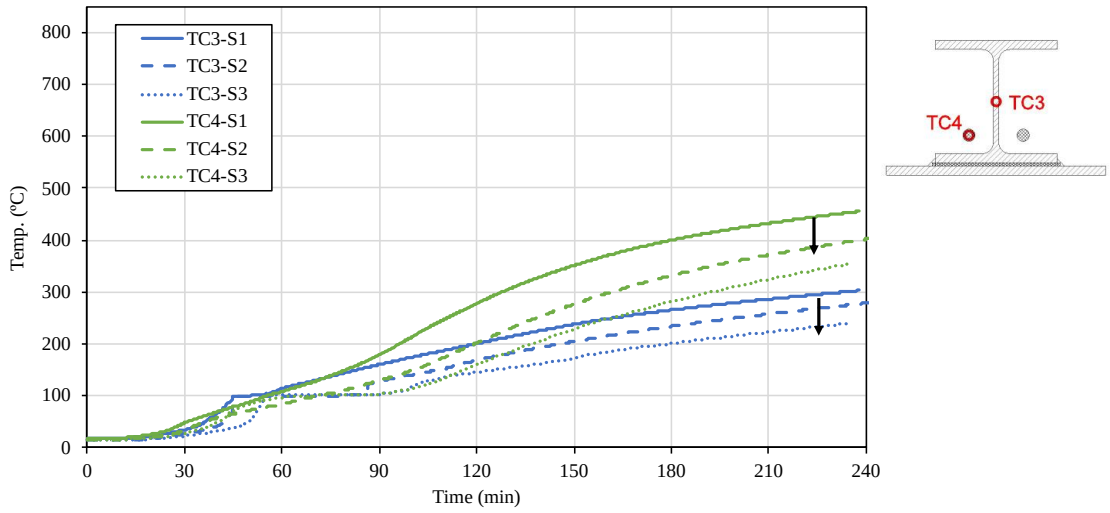

Fig. 9. Evolution of the measured temperatures along the fire exposure time: a) TC1-TC2, b) TC3-TC4.

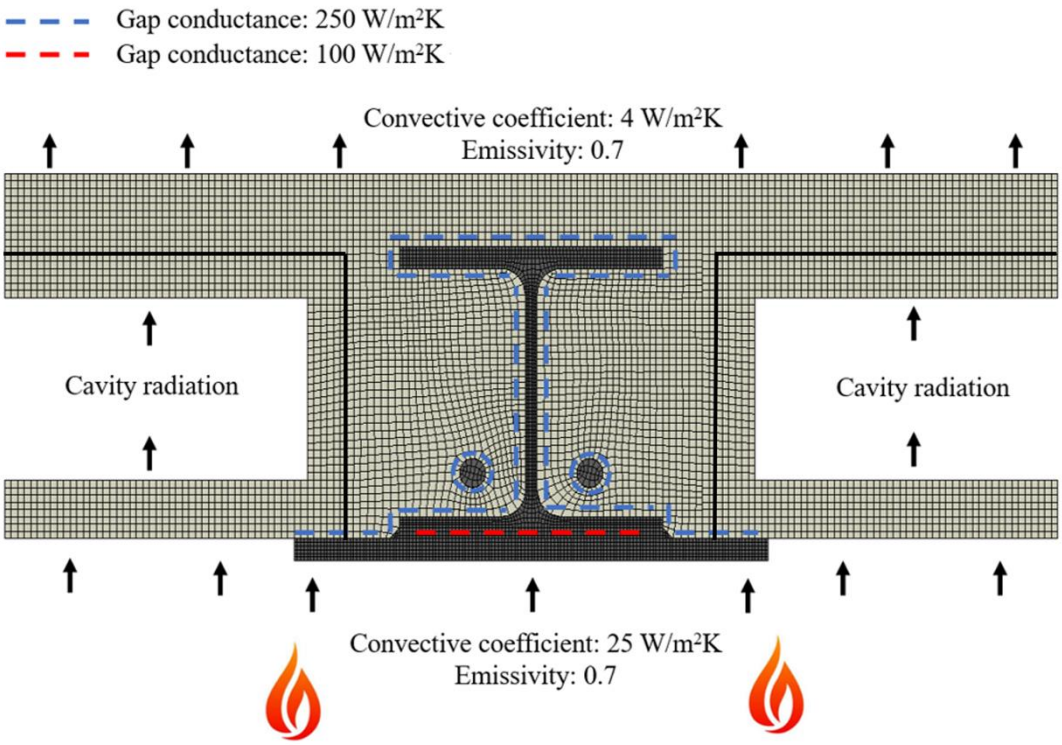

Fig. 10. FE thermal model. Mesh and boundary conditions [16]

a)

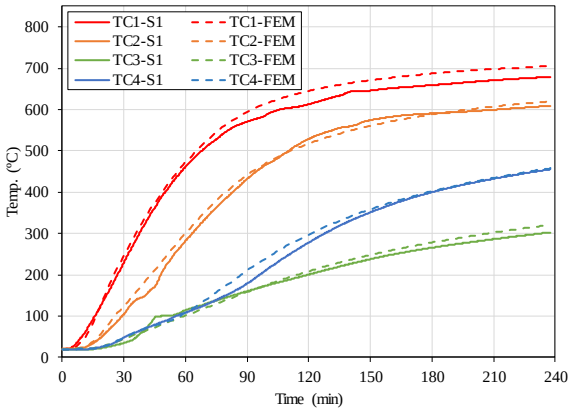

b)

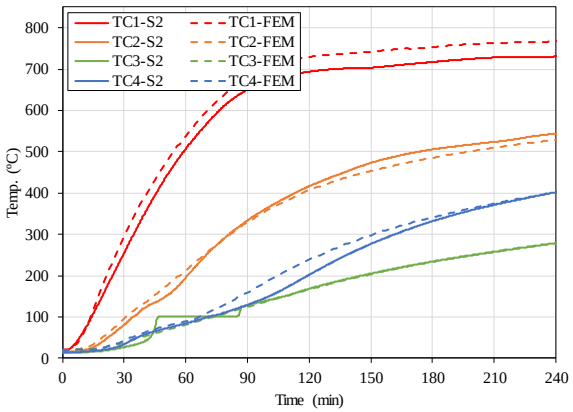

c)

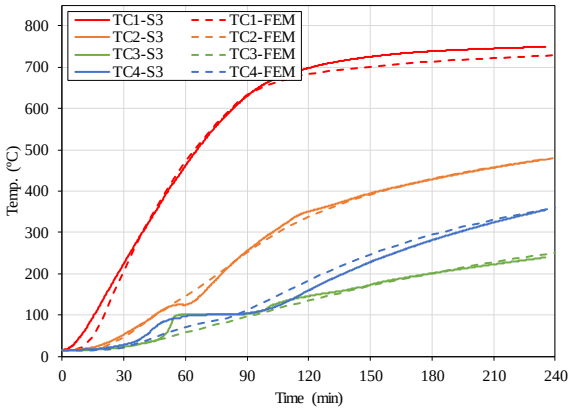

Fig. 11. Comparison between numerical (FEM) and experimental results: a) S1; b) S2; c) S3

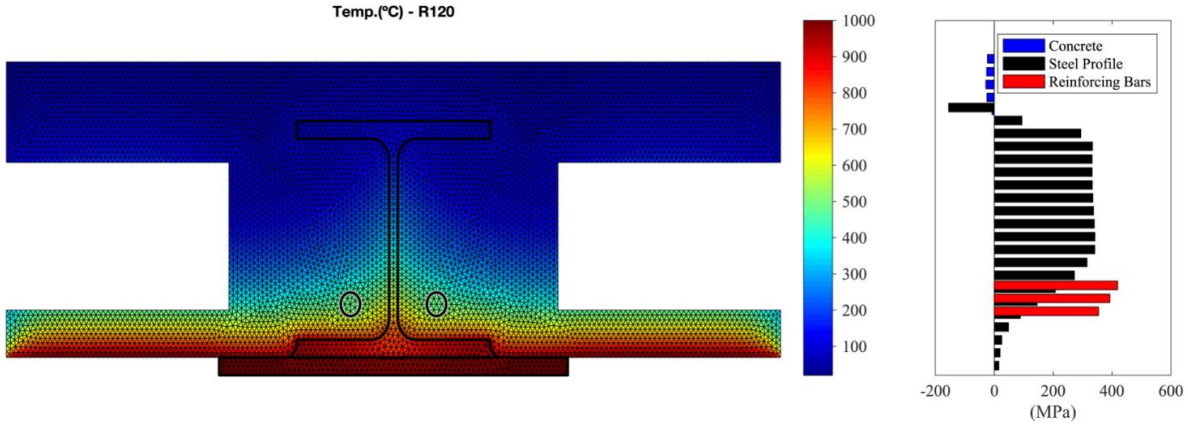

Fig. 12. Temperature and stress distribution along slim-floor cross-section after 120 minutes of standard fire exposure [8].

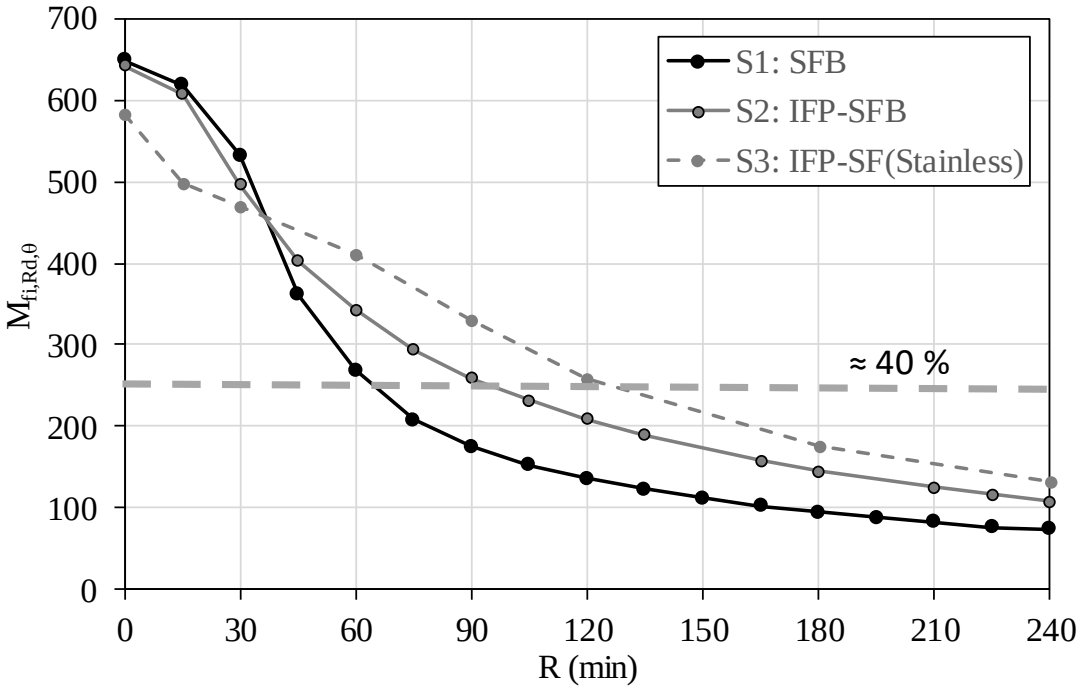

Fig. 13. Bending resistance evolution under ISO834 time-temperature fire curve.

Table 1. Specimen list

Specimen ID	**Description**
S1	SFB: HEB200 + Plate 15
S2	IFP-SFB: HEB200 + Plate 15 + **Insulation Layer**
S3	IFP-SFB: HEB200 + Plate 15 (**Stainless steel**) + **Insulation Layer**

Table 2. Experimental and FEM results (Temperature in ºC)

Time (min)	**TF**	**TC1 exp/num**	**TC2 exp/num**	**TC3 exp/num**	**TC4 exp/num**
			Test S1		
0	21	21/21	21/21	21/21	21/21
30	571	229/247	104/125	35/44	48/48
60	698	461/472	282/301	114/101	108/108
90	748	571/594	432/441	160/158	179/210
120	760	613/645	529/518	200/208	278/298
150	766	646/671	574/560	238/248	351/358
180	770	659/687	590/588	265/278	400/402
210	772	671/698	599/607	286/302	432/434
240	774	679/705	609/620	303/321	455/457
			Test S2		
0	21	21/21	21/21	21/21	21/21
30	561	255/295	81/95	27/38	34/43
60	698	507/539	196/213	100/81	84/89
90	772	650/679	334/329	128/124	129/160
120	798	694/729	416/406	168/167	201/238
150	798	703/742	473/454	205/203	276/298
180	801	717/753	506/485	234/234	332/341
210	802/	728/763	524/510	257/258	371/374
240	802	731/767	545/529	280/280	404/403
			Test S3		
0	15	15/15	15/15	15/15	15/15
30	557	225/208	53/47	23/22	28/22
60	711	461/471	124/145	-/58	97/71
90	780	631/632	255/252	103/96	104/112
120	785	698/683	350/338	146/135	160/184
150	786	725/701	395/392	173/171	228/247
180	789	739/714	429/429	201/202	281/294
210	790	745/722	457/458	223/228	324/331
240	790	749/729	477/480	239/250	354/360
Mean error num/exp (ξ)		*1.03*	*1.02*	*1.02*	*1.05*
				Total error (ξ)	**1.03**

Table 3. Plastic bending resistance under ISO834 fire exposure.

fire exposure time (min)	**S1** $M_{pl,Rd,\theta}$ (m ·kN)	**S2** $M_{pl,Rd,\theta}$ (m ·kN)	**S3** $M_{pl,Rd,\theta}$ (m ·kN)
0	648,9	642,5	583,5
30	532,5	496,1	469,3
60	268,5	343,2	411,7
90	175,5	258,8	330,5
120	135,8	209,3	259,2
180	95,0	145,2	176,1
240	73,8	108,0	131,3